

# Microwave driven geometric quantum computation on semiconductor charge qubits

Chengxian Zhang,<sup>1</sup> Tao Chen,<sup>1</sup> Xin Wang,<sup>2,3</sup> and Zheng-Yuan Xue<sup>1,4,\*</sup>

<sup>1</sup>Guangdong Provincial Key Laboratory of Quantum Engineering and Quantum Materials, and School of Physics and Telecommunication Engineering, South China Normal University, Guangzhou 510006, China

<sup>2</sup>Department of Physics, City University of Hong Kong, Tat Chee Avenue, Kowloon, Hong Kong SAR, China

<sup>3</sup>City University of Hong Kong Shenzhen Research Institute, Shenzhen, Guangdong 518057, China

<sup>4</sup>Frontier Research Institute for Physics, South China Normal University, Guangzhou 510006, China

(Dated: April 2, 2020)

The charge qubit based on semiconductor double quantum dots is promising to realize fast and scalable quantum information processing. However, due to its strong coupling to charge noise, experimental realization of two-qubit gates has fidelities below 90%. Here, we provide a theoretical framework to achieve precise gate operations on a charge qubit using geometric quantum phase, namely geometric quantum gates. Single-qubit operations are implemented using the microwave-driven X-Y interacting Hamiltonian near certain sweet spots, where the charge noise is effectively suppressed. Meanwhile, we find that the performance of the geometric gates can be further improved up to 99.86% using composite pulses. In addition, to obtain a nontrivial two-qubit gate, we introduce a hybrid system which consists of charge qubits interacting with a high-impedance superconducting resonator. We find that when the individual charge qubit is in resonance with the resonator, it is possible to construct a SWAP-like gate with fidelity over 97%. Therefore, our results suggest that the geometric quantum gates in combination with the microwave-driven fields are powerful tools to achieve high-fidelity manipulation for the charge qubit.

## I. INTRODUCTION

Semiconductor-based quantum-dot charge qubit [1–6] is a promising candidate to realize fast universal quantum computation, thanks to its large energy-level splitting which speeds up the gates. However, high-fidelity manipulation of the charge qubit remains a key challenge because of its strong coupling to the charge noise. Several theoretical approaches have been proposed to mitigate the noise effects and improve the gate fidelity, for example, the pulse engineering [7] and dynamically corrected gates [8–12]. However, these methods focus on suppressing noises in the dynamical process, which is sensitive to local noise fluctuations. Recently, it has been demonstrated that strongly microwave-driven operations near certain sweet spots can effectively suppress the general  $1/f$  charge noise [4, 6, 13–16]. Despite these progresses, experimental realization of two-qubit gates still have fidelities below 90% [4]. Therefore, further improving the gate fidelity and enhancing its robustness against noises is key for quantum computation with semiconductor charge qubits.

Beside the dynamical correction schemes mentioned above, implementation of quantum gates using geometric phases [17–19] is believed to be an effective alternative to realize high-fidelity quantum computation [20, 21]. This is owing to the fact that geometric phases have global properties, namely, it is determined only by the closed path of a cyclic evolution and therefore is robust to certain types of local noises. Therefore, much attention has been paid to geometric quantum gates (GQGs), which can be realized based on either the adiabatic [20–29] or non-adiabatic [30, 31] evolutions. Particularly, the non-adiabatic GQG is of great interest compared to the adiabatic approach, the latter of which requires an overly long

gating time that is impractical in experiments. Thus, here we focus on the non-adiabatic GQGs, which has been realized in various systems using Abelian [32–38] or non-Abelian [24, 39–51] geometric phases of quantum states. In fact, the Abelian and non-Abelian geometric phases are related by a phase factor and a holonomic matrix [52]. In addition, GQG has also been investigated in the context of semiconductor quantum dots using spin states [38, 53–57] and charge states [34, 55, 58, 59], based on non-adiabatic evolutions. Nevertheless, GQG in combination with the optimization techniques, especially microwave-driven operation near the sweet spot, is still lacking.

Here, we present a theoretical framework to implement universal GQGs for the charge qubit. To implement arbitrary single-qubit GQGs, we adopt the X-Y interacting Hamiltonian of two-level systems [35–38, 60, 61]. The path of evolution is divided into three distinct parts such that the dynamical phase is cancelled out, leaving only the geometric phase. Typically, for the semiconductor charge qubit, an efficient way to obtain the X-Y interacting Hamiltonian is to introduce a strongly microwave-driven oscillating pulsing on the detuning near the sweet spot, which has also been demonstrated in several recent experiments [4, 14, 62, 63]. It is shown that in the rotating frame and under the rotating-wave approximation, the detuning noise can drop out and only the tunneling noise in the  $\sigma_z$  term remains. Meanwhile, we have analytically demonstrated that this gate can be further improved by incorporating the composite pulses technique. In addition, to quantitatively evaluate the gate performance of the composite pulses, we perform randomized benchmarking (RB) of the GQGs. We find that the gate fidelities of the composite pulses can be as high as 99.86%.

On the other hand, scalable quantum information processing requires coupling between adjacent qubits. Recently, experiments have shown great progresses of imposing strong and long-range coupling between charge qubits via virtual mi-

\*Electronic address: [zyxue83@163.com](mailto:zyxue83@163.com)

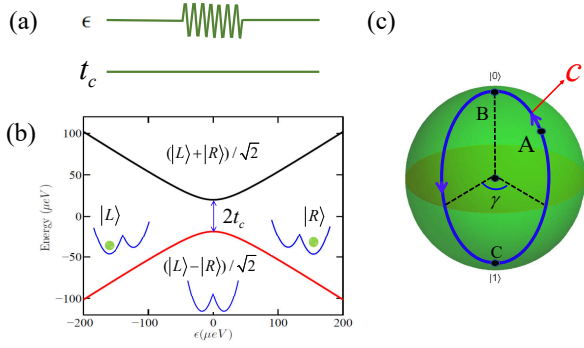


FIG. 1: Illustration of the GQG implementation based on charge qubit. (a) Microwave-driven pulse on the detuning near the sweet spot ( $\bar{\epsilon} = 0$ ) while the tunneling is fixed. (b) Energy level diagram of the charge qubit. In the regime  $\epsilon \gg t_c$ , the eigenstates are the position states  $|L\rangle$  and  $|R\rangle$  while they are the asymmetric and symmetric states  $\{|0\rangle = (|L\rangle - |R\rangle)/\sqrt{2}, |1\rangle = (|L\rangle + |R\rangle)/\sqrt{2}\}$  near the sweet spot (namely,  $\epsilon \ll t_c$ ). (c) The evolution path of state  $|+\rangle$ . The geometric phase can be achieved through the cyclic evolution along the path A-B-C-A.

crowave photons of high-impedance SQUID array resonators [64]. The total Hamiltonian of the hybrid system consisting of the charge qubits and the resonator can be described by the well-known Tavis-Cummings model [65]. When both qubits and the resonator are in resonance, this Hamiltonian in the single excitation subspace forms an effective three-level  $\Lambda$  structure, which can be used to construct a non-Abelian two-qubit gate [66], i.e., A Non-Abelian SWAP-like GQG. By numerically solving the quantum master equation, we find that the gate fidelities exceed 97%. Furthermore, we demonstrate that this gate is actually entangling, able to generate maximally entangled states. Therefore, our results suggest that high-fidelity universal GQGs on charge qubits can be achieved in combination with the microwave-driven field.

## II. SINGLE-QUBIT GQG

We first show how an arbitrary single-qubit GQG is implemented on the charge qubit. As shown in Fig. 1(b), a single electron confined in the double quantum dots (DQD) can occupy either the left (L) or right (R) dot, corresponding to position states labeled by  $|L\rangle$  and  $|R\rangle$  respectively. In the absence of noise, the Hamiltonian [64] of this two-level system reads

$$H_0 = t_c \tau_x - \frac{\epsilon}{2} \tau_z, \quad (1)$$

where  $\tau_x$  and  $\tau_z$  are the Pauli matrices in the position states spanned by  $\{|L\rangle, |R\rangle\}$ , while  $\epsilon$  and  $t_c$  are the on-site energy difference (detuning) and tunneling, respectively. Here, we define the computational bases using the asymmetric and symmetric states  $\{|0\rangle = (|L\rangle - |R\rangle)/\sqrt{2}, |1\rangle = (|L\rangle + |R\rangle)/\sqrt{2}\}$  rather than the conventional position states (to be explained later). While it is straightforward to use square-pulsed gate (DC

signal) in the experiment, it is better to perform microwave-driven gating (AC signal) near the sweet spot ( $\bar{\epsilon} = 0$ ) which is first-order insensitive to the charge noise [16]. In this way, we have  $\epsilon = 2A_\epsilon(t) \cos(\omega t + \varphi)$  where  $A_\epsilon(t)$  is the time-dependent amplitude and  $\varphi$  is the phase of the AC field. When  $2t_c$  matches the resonance frequency  $\omega$  and  $\omega \gg \delta\epsilon, A_\epsilon$ , in the rotating frame and under the rotating wave approximation (see Appendix. A), the effective Hamiltonian in the computational bases becomes

$$H_{\text{rot}}(t) = \frac{A_\epsilon(t)}{2} (\cos\varphi \sigma_x + \sin\varphi \sigma_y), \quad (2)$$

where  $\sigma_x$  and  $\sigma_y$  are the Pauli matrices in the computational bases. From Eq. (2), one is able to implement arbitrary gate operations (dynamical gates) on the  $x - y$  plane and the rotating axis is determined by  $\varphi$ . On the other hand,  $H_{\text{rot}}$  is elementary to realize universal single-qubit GQG. To do so, the entire evolution time is divided into three parts. In each part, the control amplitude meets the requirements of

$$\begin{aligned} \int_0^{T_1} A_\epsilon(\tau) d\tau &= \theta, & \left\{ \varphi_1 = \varphi - \frac{\pi}{2}, \tau \in [0, T_1] \right\}, \\ \int_{T_1}^{T_2} A_\epsilon(\tau) d\tau &= \pi, & \left\{ \varphi_2 = \varphi + \gamma - \frac{\pi}{2}, \tau \in [T_1, T_2] \right\}, \\ \int_{T_2}^T A_\epsilon(\tau) d\tau &= \pi - \theta, & \left\{ \varphi_3 = \varphi - \frac{\pi}{2}, \tau \in [T_2, T] \right\}, \end{aligned} \quad (3)$$

which leads to the arbitrary single-qubit gate of

$$U_s(T, \gamma) = U_s(T, T_2) U_s(T_2, T_1) U_s(T_1, 0) = e^{i\gamma \vec{n} \cdot \vec{\sigma}}, \quad (4)$$

where  $\vec{n} = (\sin\theta \cos\varphi, \sin\theta \sin\varphi, \cos\theta)$  is the unit vector and  $\vec{\sigma} = (\sigma_x, \sigma_y, \sigma_z)$ . The total evolution time for arbitrary gate is the same and is determined by  $\int_0^T A_\epsilon(\tau) d\tau = 2\pi$ . Since  $\gamma, \theta$  and  $\varphi$  can be controlled independently via the microwave field, it is convenient to operate arbitrary rotation on the Bloch sphere.

To see why  $U_s(T, \gamma)$  is a pure geometric gate, we consider a pair of orthogonal states

$$\begin{aligned} |+\rangle &= \cos\frac{\theta(t)}{2} |0\rangle + \sin\frac{\theta(t)}{2} e^{i\varphi(t)} |1\rangle, \\ |-\rangle &= \sin\frac{\theta(t)}{2} e^{-i\varphi(t)} |0\rangle - \cos\frac{\theta(t)}{2} |1\rangle. \end{aligned} \quad (5)$$

At the final time  $T$ , the orthogonal states under the operation of  $U_s(T, \gamma)$  acquire a global phase factor, namely, the Abelian phase:  $|\pm\rangle \rightarrow e^{\pm i\gamma} |\pm\rangle$ . Thus, in the orthogonal bases the operator can be written as  $U_s(T, \gamma) = e^{i\gamma} |+\rangle \langle +| + e^{-i\gamma} |-\rangle \langle -|$ . In fact,  $\gamma$  is a pure GPs in the parameter space defined by this orthogonal states. As shown in Fig. 1(c), the evolution path of  $|+\rangle$  can be described by a continuous curve  $\mathcal{C} : t \in [0, T]$  on the Bloch sphere. It starts at a given point A. By setting  $\theta(T) = \theta(0)$  and  $\varphi(T) = \varphi(0)$ , curve  $\mathcal{C}$  encloses a closed loop on the sphere. Since  $\varphi$  is fixed in each part of the evolution,  $|+(t)\rangle$  evolves along the geodesic line and the dynamical phase is cancelled out, only

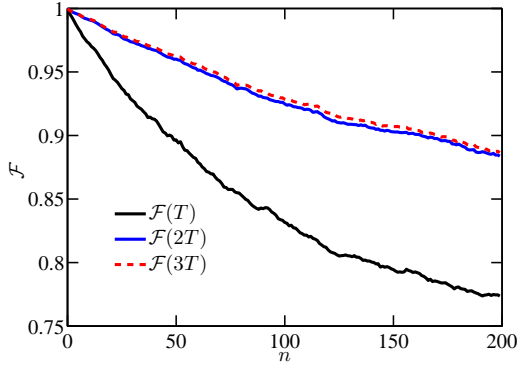


FIG. 2: Numerical RB of the GQG as a function of the Clifford gate number. The black solid line denotes the gate fidelity for the original geometric gate  $U_s(T, \gamma)$ , while the solid blue and dashed red lines indicate the results for  $U(2T, \gamma/2)$  and  $U(3T, \gamma/3)$ , respectively.

the geometric phase remains [38].

Next, we show the robustness of the GQGs to the charge noise. For the microwave-driven charge qubits, the AC field can also introduce potential driving effects that could result gate errors [16], such as the Bloch-Siegert shift of the resonant frequency [67] and errors in the Rabi frequency [13, 68], both of which can lead to dephasing. Whereas, they can be mitigated and accommodated by several approaches including employing AC sweet spot [69] or pulse engineering [15, 70]. Thus, we neglect this driving effect and focus only on the charge noise. Charge noise shifts both the detuning and tunneling values, namely,  $\epsilon \rightarrow \epsilon + \delta\epsilon$  and  $t_c \rightarrow t_c + \delta t_c$  where  $\delta t_c$  and  $\delta\epsilon$  are regarded as static random variables. Hereafter, we regard  $\delta\epsilon$  and  $\delta t_c$  as the detuning noise and tunneling noise, respectively. Under the rotating-wave approximation, we find that only the tunneling noise in the  $\sigma_z$  term of the effective Hamiltonian remains while the detuning noise can be safely ignored (see Appendix A). The evolution operator reads

$$R(\gamma) = \exp \left[ -i (H_{\text{rot}} + \delta t_c \sigma_z) \frac{\gamma}{A_\epsilon} \right]. \quad (6)$$

To demonstrate the superiority of the GQG we perform its numerical RB [71, 72]. The RB is simulated by averaging the gate fidelity over different noise and gate sequences randomly drawn from the single-qubit Clifford group [73, 74]. We consider the detuning noise  $\delta\epsilon$  and tunneling noise  $\delta t_c$  are drawn randomly from the Gaussian distribution  $\sigma_t^2 : \mathcal{N}(0, \sigma_t^2)$  and  $\sigma_\epsilon^2 : \mathcal{N}(0, \sigma_\epsilon^2)$ , where the mean value of the noise is zero and  $\sigma_t$  ( $\sigma_\epsilon$ ) is related to the standard deviation. For convenience, we also assume the magnitudes of these two deviations are the same, namely  $\sigma_t = \sigma_\epsilon$ . In Ref. [16], the deviation can be calculated via  $\sigma_\epsilon = c_\epsilon [2 \ln(\sqrt{2\pi} c_\epsilon / \hbar \omega_l)]^{1/2}$ , where  $\omega_l$  is the cutoff frequency and  $c_\epsilon$  is the related parameter to the deviation. We take  $c_\epsilon = 0.5 \mu\text{eV}$  and  $\omega_l/2\pi = 1\text{Hz}$  such that  $\sigma_t = \sigma_\epsilon \approx 3 \mu\text{eV}$ . In Fig. 2, we plot the fidelity as a function of the Clifford gate number. The averaged gate fidelity is obtained by fitting the fidelity curve to  $(1 + e^{-dn})/2$ . We find that the gate fidelity  $\mathcal{F}(T)$  related to  $U_s(T, \gamma)$  is 99.63%.

The fidelity of the achieved GQG can be further improved using a scheme involving composite pulses. The basic idea is to divide the original rotation into several parts, such that the sensitiveness of the composite GQG can be different. To show the advanced superiority of the composite scheme, we consider two- and three-piece composite pulses with the corresponding evolution operator as

$$\begin{aligned} U(2T, \gamma/2) &= U_s(T, \gamma/2) \cdot U_s(T, \gamma/2), \\ U(3T, \gamma/3) &= U_s(T, \gamma/3) \cdot U_s(T, \gamma/3) \cdot U_s(T, \gamma/3). \end{aligned} \quad (7)$$

In the assumption of  $\delta t_c \ll 1$ , We expand the fidelities to second-order as

$$\begin{aligned} \mathcal{F}^2(T) &= 1 + (8 \cos \gamma - \cos 2\gamma - 2 \cos 2\theta \sin^2 \gamma - 7) \delta t_c^2, \\ \mathcal{F}^2(2T) &= 1 + \{4 (\cos \gamma/2 - 3) (\sin \gamma/4 - \sin 3\gamma/4)^2 \\ &\quad - 2 \cos 2\theta \sin^2 \gamma\} \delta t_c^2, \\ \mathcal{F}^2(3T) &= 1 + \{(\sin \gamma/6 - \sin \gamma/2 + \sin 5\gamma/6)^2 \times \\ &\quad 4 (\cos \gamma/3 - 3) - 2 \cos 2\theta \sin^2 \gamma\} \delta t_c^2. \end{aligned} \quad (8)$$

Further, we have

$$\begin{aligned} \Delta \mathcal{F}_1 &= \mathcal{F}^2(2T) - \mathcal{F}^2(T) \\ &= 64(1 + 2 \cos \gamma/2) \sin^4(\gamma/4) \delta t_c^2, \\ \Delta \mathcal{F}_2 &= \mathcal{F}^2(3T) - \mathcal{F}^2(2T) \\ &= 64(1 + 2 \cos \gamma/6 + 2 \cos \gamma/3) \times \\ &\quad (-1 + 2 \cos \gamma/3 + 2 \cos \gamma/2)^2 \sin^4(\gamma/12) \delta t_c^2. \end{aligned} \quad (9)$$

It is easy to find that for arbitrary rotation angle within  $-\pi \leq \gamma \leq \pi$  we always have  $\Delta \mathcal{F}_1 \geq 0$  and  $\Delta \mathcal{F}_2 \geq 0$ . This means the composite GQG do offer fidelity improvement. From the RB result in Fig. 2, we find that both the composite schemes can outperform the original GQG. Also, we see that the improvement offered by  $U(2T, \gamma/2)$  with respect to  $U(T, \gamma)$  is substantial, while the improvement of  $U(3T, \gamma/3)$  over  $U(2T, \gamma/2)$  is marginal, where the fidelities are 99.85% and 99.86%, respectively.

### III. NONTRIVIAL TWO-QUBIT GQG

To implement the two-qubit GQG we consider two DQDs strongly coupled via one of its plunger gates to a high-impedance SQUID array superconducting resonator [64]. The high-impedance resonator enhances the coupling strength of the individual qubits to the resonator. For this coupled system, the Hamiltonian reads

$$H_{\text{tot}} = H_{\text{res}} + \sum_k H_k + \sum_k H_{\text{int},k}, \quad (10)$$

with the resonator Hamiltonian  $H_{\text{res}} = \omega_r a^\dagger a$ , where  $\omega_r$  is the resonant angular frequency of the superconducting resonator,  $H_k$  is the charge qubit Hamiltonian as shown in Eq. (1) for the  $k$ th DQD ( $k = 1, 2$ ) and the coupling between resonator and DQDs reads  $H_{\text{int},k} = g_k \tau_k^z (a^\dagger + a)$ . Here,  $a$  ( $a^\dagger$ )

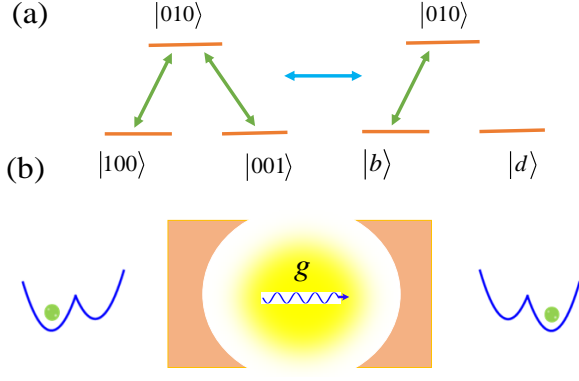


FIG. 3: Implementation of the two-qubit GQG. (a) When both qubits and the resonator are resonant, they form a three-level  $\Lambda$  system with the transition between  $|100\rangle \leftrightarrow |010\rangle$  and  $|001\rangle \leftrightarrow |010\rangle$ . In the dark and bright representation the dark state decouples the system. (b) Diagram of the charge qubits and resonator coupled system.

is the bosonic annihilation (creation) operator and  $g_k$  is the dipolar coupling strength between the  $k$ th DQD and the resonator. In order to simulate the well-known Tavis-Cummings Hamiltonian, we transform the coupled Hamiltonian into the DQD eigenbasis spanned by  $\{|g\rangle, |e\rangle\}$  as

$$H_{\text{tot}} = \omega_r a^\dagger a - \frac{1}{2} \sum_k \omega_k \tilde{\sigma}_k^z + g_k \sum_k \sin \theta_k (a^\dagger \tilde{\sigma}_k + h.c.),$$

where we have used rotating-wave approximation,  $\omega_k = \sqrt{(4t_c^k)^2 + \epsilon^2}$ ,  $\tan \theta_k = 2t_c^k/\epsilon_k$  and  $\sin \theta_k = 2t_c^k/\omega_k$ . Note that since we have rewritten the Hamiltonian in the DQDs eigenstates, such that the Pauli matrices here are  $\tilde{\sigma}_k^z = |g\rangle\langle g| - |e\rangle\langle e|$ ,  $\tilde{\sigma}_k = |g\rangle\langle e|$  and  $(\tilde{\sigma}_k)^\dagger = |e\rangle\langle g|$ . We can also find that the effective coupling strength is  $g_k \sin \theta_k$ , which is affected by a factor of  $\sin \theta_k$ . Experimentally,  $g_k$  is difficult to change, and thus we assume it to be fixed. On the other hand,  $\sin \theta_k$  is determined by the qubit operating parameters, namely,  $\epsilon$  and  $t_c^k$ . In the limit  $\epsilon \gg t_c^k$ , the eigenstates are approximately the position states  $|L\rangle$  and  $|R\rangle$ , and we have  $\sin \theta_k = 2t_c^k/\omega_k \approx 2t_c^k/\epsilon_k$ . In this case, the effective coupling can be very small. Inversely, in the limit  $\epsilon \ll t_c^k$ , the eigenstates are approximately the symmetric and asymmetric states  $(|L\rangle + |R\rangle)/\sqrt{2}$  and  $(|L\rangle - |R\rangle)/\sqrt{2}$  and  $\sin \theta_k \approx 1$ . To obtain a large effective coupling, one can operate the qubit in this region. This can be realized by taking  $t_c^1 = t_c^2$  to be fixed and operating  $\epsilon$  near the sweet spot, where the qubit dephasing is improved.

Next, we transform  $H_{\text{tot}}$  into the rotating frame defined by the resonant frequency  $\omega_r$ . The effective Hamiltonian reads

$$H_{\text{eff}} = U^\dagger H_{\text{tot}} U - iU^\dagger \frac{\partial U}{\partial t} = \frac{1}{2} \sum_k \Delta_k \sigma_k^z + \sum_k g_k \sin \theta_k (a^\dagger \sigma_k + h.c.), \quad (11)$$

with

$$U = e^{-i\omega_r (a^\dagger a - \sum_k \frac{1}{2} \sigma_k^z) t}, \quad \Delta_k = \omega_r - \omega_k. \quad (12)$$

Considering both DQDs and the resonator are resonant, namely,  $\omega_k = \omega_r$ , the effective Hamiltonian becomes

$$H_{\text{eff}} = \sum_k g_k a^\dagger \sigma_k + h.c., \quad (13)$$

where we have assumed  $\sin \theta_k = 1$  and thus the Pauli matrices  $\tilde{\sigma}$  is equivalent to  $\sigma$  and therefore  $|e\rangle = |1\rangle$  and  $|g\rangle = |0\rangle$ . In the single excitation subspace spanned by  $\{|100\rangle, |010\rangle, |001\rangle\}$  (where  $|mnq\rangle \equiv |m_1\rangle |n_r\rangle |q_2\rangle$  denoting the first qubit, the resonator and the second qubit, in an order from left to right), the Hamiltonian in Eq. (13) actually forms a three-level system with the transition between  $|100\rangle \leftrightarrow |010\rangle$  and  $|001\rangle \leftrightarrow |010\rangle$ , as shown in Fig. 3(a). Under the dressed state representation, the effective Hamiltonian is

$$H_{\text{eff}} = g_1 |010\rangle \langle 100| + g_2 |010\rangle \langle 001| + h.c. = \Omega |010\rangle \langle b| + h.c., \quad (14)$$

with the dark and bright dressed states being

$$|b\rangle = \sin \frac{\theta}{2} e^{-i\phi} |0\rangle - \cos \frac{\theta}{2} |1\rangle, \\ |d\rangle = \cos \frac{\theta}{2} |0\rangle + \sin \frac{\theta}{2} e^{i\phi} |1\rangle, \quad (15)$$

where  $\Omega = \sqrt{g_1^2 + g_2^2}$ ,  $\tan \theta/2 = g_1/g_2$ . It is clear from Eq. (14) that the dark state  $|d\rangle$  decouples from the dynamics and the Hamiltonian can be regarded as oscillating between the bright state  $|b\rangle$  and  $|010\rangle$ . Thus,  $|b\rangle$  and  $|d\rangle$  evolve as

$$|\psi_1(t)\rangle = U_{\text{eff}}(t) |d\rangle = |d\rangle \\ |\psi_2(t)\rangle = U_{\text{eff}}(t) |b\rangle = \cos(\Omega t) |b\rangle - i \sin(\Omega t) |010\rangle,$$

where  $U_{\text{eff}} = \exp(\int_0^T H_{\text{eff}} dt)$ . When  $\Omega T = \pi$  is satisfied, these two dressed states undergo a cyclic evolution with  $|\psi_i(T)\rangle \langle \psi_i(T)| = |\psi_i(0)\rangle \langle \psi_i(0)|$ , ( $i = 1, 2$ ). The dark state  $|d\rangle$  remains the same while the bright state  $|b\rangle$  acquires a  $\pi$  phase factor and thus turns to  $-|b\rangle$ . Under the subspace  $\{|d\rangle, |b\rangle, |010\rangle\}$  the evolution operator is

$$U_{\text{eff}}(T) = \sum_{i,j=1}^2 \left[ \hat{T} e^{i \int_0^T [A(t) - H_{\text{eff}}] dt} \right]_{i,j} |\psi_i(0)\rangle \langle \psi_j(0)|, \quad (17)$$

with  $A_{ij}(t) = i \langle \psi_i(t) | \dot{\psi}_j(t) \rangle$ . Besides, it is easy to find that  $\langle \psi_i(t) | H_{\text{eff}} | \psi_j(t) \rangle = 0$  which means there is no transition between  $|\psi_1(t)\rangle$  and  $|\psi_2(t)\rangle$ , namely, the parallel-transport condition is satisfied. Thus,  $U_{\text{eff}}(T)$  represents a non-Abelian (holonomic) two-qubit GQG. Furthermore, under the logical

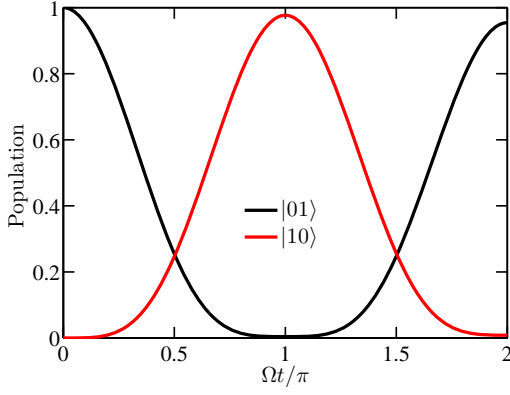


FIG. 4: State populations of  $|100\rangle$  and  $|001\rangle$  versus the evolution time. The fidelity is obtained by calculated the population of  $|001\rangle$  when  $\Omega t = \pi$ .

basis states  $\{|00\rangle, |01\rangle, |10\rangle, |11\rangle\}$  it takes the form of

$$U_2(\xi) = \begin{pmatrix} 1 & 0 & 0 & 0 \\ 0 & \cos \xi & \sin \xi & 0 \\ 0 & \sin \xi & -\cos \xi & 0 \\ 0 & 0 & 0 & -1 \end{pmatrix} \quad (18)$$

where  $\xi = 2 \arctan(g_1/g_2)$ . For the simplest case where  $g_1 = g_2$  such that  $\xi = \pi/2$  we can get a SWAP-like two-qubit gate

$$U_{\text{SWAP}} = \begin{pmatrix} 1 & 0 & 0 & 0 \\ 0 & 0 & 1 & 0 \\ 0 & 1 & 0 & 0 \\ 0 & 0 & 0 & -1 \end{pmatrix}. \quad (19)$$

Note that the negative sign in the elements  $|11\rangle \langle 11|$  comes from the evolution of the dual excitation subspace of  $\{|110\rangle, |101\rangle, |011\rangle\}$  [66]. That is because in this subspace it can also form another three-level system (see Appendix B) with the transition between  $|110\rangle \leftrightarrow |101\rangle$  and  $|011\rangle \leftrightarrow |101\rangle$ . We can show that  $U_{\text{SWAP}}$  is actually a perfect entangling gate, namely, it can generate maximally entangled states, see Appendix C.

Then, we simulate the performance of this two-qubit entangling gate using the Lindblad master equation of

$$\dot{\rho} = i[\rho, H_{\text{tot}}] + \frac{\kappa}{2}\mathcal{L}(a) + \frac{\Gamma}{2}\mathcal{L}(\sigma_1^z + \sigma_2^z), \quad (20)$$

where  $\rho$  is the density matrix of the coupled system,  $\mathcal{L}(A) = 2A\rho A^\dagger - A^\dagger A\rho - \rho A^\dagger A$  is the Lindblad operator;  $\kappa$  and  $\Gamma$  are the decay and dephasing rate of the resonator and the qubits, respectively. As stated before, when the charge qubits are operated near the sweet spot using the microwave-driven field, the charge noise exists only in the  $\sigma_z$  term, therefore, the leading error for the charge qubit is pure dephasing caused by the tunneling noise. According to Ref. [64], we consider the coupling strength to be  $g/2\pi = 60$  MHz and the decay and dephasing rate are  $\kappa/2\pi = \Gamma/2\pi = 6$  MHz. Normally, the fidelity can be calculated via  $F_{\text{SWAP}} = \text{Tr}[\rho_{\text{id}}(t)\rho(t)]$ , where  $\rho(t)$  is the density matrix within time and  $\rho_{\text{id}}(t)$  is the

ideal density matrix. Thus, for a given initial density operator (state), one can obtain  $\rho(t)$  by solving the master equation and then calculate the fidelity. Alternatively, the fidelity can also be obtained by calculating the population of the considered state. Here, we consider the initial state of the coupled system is  $|100\rangle$ , i.e.  $|e, 0, g\rangle$ . Under the operation of  $U_{\text{SWAP}}$ , it is expected to transform to  $|001\rangle$  in the absence of dephasing and decay. In Fig. 4, we plot the populations of the state  $|100\rangle$  and  $|001\rangle$  versus the evolution time. We find that the population (fidelity) for  $|001\rangle$  is 97.68% when  $\Omega t = \pi$ .

#### IV. CONCLUSION

In conclusion, we have proposed the implementation of universal GQG for the charge qubit. We introduce the microwave-driven field operating on the sweet spot and obtain the X-Y interacting Hamiltonian. By dividing the evolution path into three distinct parts, we are able to obtain universal Abelian single-qubit gates. Furthermore, we have applied the composite pulse technique and with that, the gate fidelity is improved above 99.8%. Meanwhile, we have designed a non-Abelian (holonomic) SWAP-like two-qubit gate and demonstrated its entangling property. By solving the master equation we have found that the related fidelity is about 97.68%. Therefore, our results offer an alternative yet powerful way to achieve high-fidelity universal geometric quantum computation for the charge qubit.

#### Acknowledgments

We thank Bao-Jie Liu for useful discussion. This work was supported by Key-Area Research and Development Program of Guangdong Province (Grant No. 2018B030326001), the National Natural Science Foundation of China (Grant No. 11905065, 11874156, 11874312), the Project funded by China Postdoctoral Science Foundation (Grant No. 2019M652928), the Research Grants Council of Hong Kong (No. CityU 11303617), and the Guangdong Innovative and Entrepreneurial Research Team Program (No. 2016ZT06D348).

#### Appendix A: Effective Hamiltonian and noise model for the single-qubit gate

For a microwave-driven charge qubit, the charge noise couples to the qubit by affecting both the detuning  $\epsilon$  and tunneling  $t_c$ . The Hamiltonian of the coupled system in the basis states spanned by  $\{|L\rangle, |R\rangle\}$  can be described by

$$H_0 = (t_c + \delta t_c)\tau_x - \frac{\epsilon + \delta\epsilon}{2}\tau_z. \quad (A1)$$

Under the computational basis states  $H_0$  can be

$$H_c = \begin{pmatrix} t_c + \delta t_c & \frac{\epsilon + \delta\epsilon}{2} \\ \frac{\epsilon + \delta\epsilon}{2} & -t_c - \delta t_c \end{pmatrix}. \quad (A2)$$

Here, we consider a microwave-driven operating on the detuning near the sweet spot  $\epsilon = 2A_\epsilon(t)\cos(\omega t + \varphi)$ . And then, we further transform  $H_c$  into the rotating frame at the microwave-field frequency  $\omega$

$$H_i = U^\dagger H_c U - iU^\dagger \frac{\partial U}{\partial t} = \begin{pmatrix} t_c + \delta t_c - \frac{\omega}{2} & \frac{\epsilon + \delta\epsilon}{2} e^{i\omega t} \\ \frac{\epsilon + \delta\epsilon}{2} e^{-i\omega t} & \frac{1}{2}(-2(t_c + \delta t_c) + \omega) \end{pmatrix}, \quad (\text{A3})$$

where  $U = \exp[-i\frac{\omega t}{2}\tau_z]$ . Considering  $\omega \gg \delta\epsilon, A_\epsilon$  and  $2t_c \sim \omega$  we have

$$H_i = \begin{pmatrix} \delta t_c & \frac{A_\epsilon}{2} e^{-i\varphi} \\ \frac{A_\epsilon}{2} e^{i\varphi} & -\delta t_c \end{pmatrix}, \quad (\text{A4})$$

where we have performed rotating wave approximation and neglected the high-frequency oscillating terms. Now, it is clear that under the microwave-driven field the detuning noise can drop out and only the tunneling noise remains.

### Appendix B: Effective Hamiltonian for the qubit-resonator coupled system

To clearly verify the evolution of the charge qubits and the resonator coupled system we write the effective Hamiltonian in the full Hilbert space

$$H_{\text{eff}} = \begin{pmatrix} 0 & g_1 & 0 & 0 & 0 & 0 & 0 & 0 \\ g_1 & \Delta & g_2 & 0 & 0 & 0 & 0 & 0 \\ 0 & g_2 & 0 & 0 & 0 & 0 & 0 & 0 \\ 0 & 0 & 0 & 0 & g_1 & 0 & 0 & 0 \\ 0 & 0 & 0 & g_1 & -\Delta & g_2 & 0 & 0 \\ 0 & 0 & 0 & 0 & g_2 & 0 & 0 & 0 \\ 0 & 0 & 0 & 0 & 0 & 0 & \Delta & 0 \\ 0 & 0 & 0 & 0 & 0 & 0 & 0 & -\Delta \end{pmatrix}, \quad (\text{A1})$$

where Eq. (A1) is in the basis states spanned by  $\{|100\rangle, |010\rangle, |001\rangle, |110\rangle, |101\rangle, |011\rangle, |000\rangle, |111\rangle\}$ . Here, we have assumed  $\Delta_1 = \Delta_2 = \Delta$ . When both the two

qubits and the resonator are resonant, namely,  $\Delta = 0$ , the Hamiltonian in the subspaces  $\{|100\rangle, |010\rangle, |001\rangle\}$  (single excitation) and  $\{|110\rangle, |101\rangle, |011\rangle\}$  (dual excitation) forms two effective three-level  $\Lambda$  structures.

### Appendix C: Demonstration of the perfect entangling gate

According to the condition in [75, 76], a perfect entangling gate  $U$  should satisfy

$$\sin^2 \varphi \leq 4|G| \leq 1 \quad (\text{A1})$$

and

$$\cos \varphi (\cos \varphi - G_3) \geq 0 \quad (\text{A2})$$

where  $G = G_1 + iG_2 = |G|e^{i\varphi}$  with

$$\begin{aligned} G_1 &= \text{Re} \left[ \frac{\text{tr}^2[m(U)]}{16} \right], \\ G_2 &= \text{Im} \left[ \frac{\text{tr}^2[m(U)]}{16} \right], \\ G_3 &= \frac{\text{tr}^2[m(U)] - \text{tr}[m^2(U)]}{4} \end{aligned} \quad (\text{A3})$$

Here,  $m(U)$  is a unitary matrix defined as

$$m(U) = (Q^\dagger U Q)^T Q^\dagger U Q, \quad (\text{A4})$$

with

$$Q = \frac{1}{\sqrt{2}} \begin{pmatrix} 1 & 0 & 0 & i \\ 0 & i & 1 & 0 \\ 0 & i & -1 & 0 \\ 1 & 0 & 0 & -i \end{pmatrix}, \quad (\text{A5})$$

where  $Q$  is the unitary transformation from the computational basis to the Bell basis. For  $U_{\text{SWAP}}$ , it is easy to find that  $G_1 = G_2 = 0$  and  $G_3 = -1$ , thus, it is a perfect entangling gate.

- 
- [1] G. Shinkai, T. Hayashi, T. Ota, and T. Fujisawa, *Phys. Rev. Lett.* **103**, 056802 (2009).
- [2] K. D. Petersson, J. R. Petta, H. Lu, and A. C. Gossard, *Phys. Rev. Lett.* **105**, 246804 (2010).
- [3] H.-O. Li, G. Cao, G.-D. Yu, M. Xiao, G.-C. Guo, H.-W. Jiang, and G.-P. Guo, *Nat. Commun.* **6**, 7681 (2015).
- [4] D. Kim, D. Ward, C. Simmons, J. K. Gamble, R. Blume-Kohout, E. Nielsen, D. Savage, M. Lagally, M. Friesen, S. Coppersmith, *et al.*, *Nat. Nanotechnol.* **10**, 243 (2015).
- [5] D. R. Ward, D. Kim, D. E. Savage, M. G. Lagally, R. H. Foote, M. Friesen, S. N. Coppersmith, and M. A. Eriksson, *Npj Quantum Inf.* **2**, 1 (2016).
- [6] Y.-C. Yang, S. N. Coppersmith, and M. Friesen, *Phys. Rev. A* **100**, 022337 (2019).
- [7] J. Emerson, *Nat. Electron.* **2**, 140 (2019).
- [8] X. Wang, L. S. Bishop, J. P. Kestner, E. Barnes, K. Sun, and S. Das Sarma, *Nat. Commun.* **3**, 997 (2012).
- [9] J. P. Kestner, X. Wang, L. S. Bishop, E. Barnes, and S. Das Sarma, *Phys. Rev. Lett.* **110**, 140502 (2013).
- [10] X. Wang, L. S. Bishop, E. Barnes, J. P. Kestner, and S. Das Sarma, *Phys. Rev. A* **89**, 022310 (2014).
- [11] X. Wang, F. A. Calderon-Vargas, M. S. Rana, J. P. Kestner, E. Barnes, and S. Das Sarma, *Phys. Rev. B* **90**, 155306 (2014).
- [12] R. E. Throckmorton, C. Zhang, X.-C. Yang, X. Wang, E. Barnes, and S. Das Sarma, *Phys. Rev. B* **96**, 195424 (2017).
- [13] C. H. Wong, *Phys. Rev. B* **93**, 035409 (2016).
- [14] J. M. Nichol, L. A. Orona, S. P. Harvey, S. Fallahi, G. C. Gardner, M. J. Manfra, and A. Yacoby, *Npj Quantum Inf.* **3**, 1 (2017).
- [15] Y.-C. Yang, S. N. Coppersmith, and M. Friesen, *Phys. Rev. A*

- 95**, 062321 (2017).
- [16] Y.-C. Yang, S. Coppersmith, and M. Friesen, *Npj Quantum Inf.* **5**, 1 (2019).
- [17] M. V. Berry, *Proc. Royal Soc. A.* **392**, 45 (1984).
- [18] F. Wilczek and A. Zee, *Phys. Rev. Lett.* **52**, 2111 (1984).
- [19] Y. Aharonov and J. Anandan, *Phys. Rev. Lett.* **58**, 1593 (1987).
- [20] J. Pachos, P. Zanardi, and M. Rasetti, *Phys. Rev. A* **61**, 010305(R) (1999).
- [21] P. Zanardi and M. Rasetti, *Phys. Lett. A.* **264**, 94 (1999).
- [22] G. Falci, R. Fazio, G. M. Palma, J. Siewert, and V. Vedral, *Nature* **407**, 355 (2000).
- [23] L.-M. Duan, J. I. Cirac, and P. Zoller, *Science* **292**, 1695 (2001).
- [24] P. Solinas, P. Zanardi, N. Zanghi, and F. Rossi, *Phys. Rev. A* **67**, 062315 (2003).
- [25] H. Wu, E. M. Gauger, R. E. George, M. Möttönen, H. Riemann, N. V. Abrosimov, P. Becker, H.-J. Pohl, K. M. Itoh, M. L. W. Thewalt, and J. J. L. Morton, *Phys. Rev. A* **87**, 032326 (2013).
- [26] K. Toyoda, K. Uchida, A. Noguchi, S. Haze, and S. Urabe, *Phys. Rev. A* **87**, 052307 (2013).
- [27] Y.-Y. Huang, Y.-K. Wu, F. Wang, P.-Y. Hou, W.-B. Wang, W.-G. Zhang, W.-Q. Lian, Y.-Q. Liu, H.-Y. Wang, H.-Y. Zhang, L. He, X.-Y. Chang, Y. Xu, and L.-M. Duan, *Phys. Rev. Lett.* **122**, 010503 (2019).
- [28] A. Frees, S. Mehl, J. K. Gamble, M. Friesen, and S. Coppersmith, *Npj Quantum Inf.* **5**, 1 (2019).
- [29] Y.-Y. Huang, Y.-K. Wu, F. Wang, P.-Y. Hou, W.-B. Wang, W.-G. Zhang, W.-Q. Lian, Y.-Q. Liu, H.-Y. Wang, H.-Y. Zhang, L. He, X.-Y. Chang, Y. Xu, and L.-M. Duan, *Phys. Rev. Lett.* **122**, 010503 (2019).
- [30] E. Sjöqvist, D. M. Tong, L. M. Andersson, B. Hessmo, M. Johansson, and K. Singh, *New J. Phys.* **14**, 103035 (2012).
- [31] G. F. Xu, J. Zhang, D. M. Tong, E. Sjöqvist, and L. C. Kwek, *Phys. Rev. Lett.* **109**, 170501 (2012).
- [32] W. Xiang-Bin and M. Keiji, *Phys. Rev. Lett.* **87**, 097901 (2001).
- [33] S.-L. Zhu and Z. D. Wang, *Phys. Rev. Lett.* **89**, 097902 (2002).
- [34] L. Wang, T. Tu, B. Gong, C. Zhou, and G.-C. Guo, *Sci. Rep.* **6**, 19048 (2016).
- [35] P. Z. Zhao, X.-D. Cui, G. F. Xu, E. Sjöqvist, and D. M. Tong, *Phys. Rev. A* **96**, 052316 (2017).
- [36] T. Chen and Z.-Y. Xue, *Phys. Rev. Appl.* **10**, 054051 (2018).
- [37] Y. Xu, Z. Hua, T. Chen, X. Pan, X. Li, J. Han, W. Cai, Y. Ma, H. Wang, Y. Song, Z.-Y. Xue, Z.-Q. Yin, and L. Sun, (2019), [arXiv:1910.12271](https://arxiv.org/abs/1910.12271).
- [38] C. Zhang, T. Chen, S. Li, X. Wang, and Z.-Y. Xue, (2020), [arXiv:2001.04855](https://arxiv.org/abs/2001.04855).
- [39] G. Feng, G. Xu, and G. Long, *Phys. Rev. Lett.* **110**, 190501 (2013).
- [40] A. A. Abdumalikov Jr, J. M. Fink, K. Juliusson, M. Pechal, S. Berger, A. Wallraff, and S. Filipp, *Nature* **496**, 482 (2013).
- [41] S. Arroyo-Camejo, A. Lazariiev, S. W. Hell, and G. Balasubramanian, *Nat. Commun.* **5**, 4870 (2014).
- [42] C. Zu, W.-B. Wang, L. He, W.-G. Zhang, C.-Y. Dai, F. Wang, and L.-M. Duan, *Nature* **514**, 72 (2014).
- [43] C. G. Yale, F. J. Heremans, B. B. Zhou, A. Auer, G. Burkard, and D. D. Awschalom, *Nat. Photonics* **10**, 184 (2016).
- [44] Y. Sekiguchi, N. Niikura, R. Kuroiwa, H. Kano, and H. Kosaka, *Nat. Photonics* **11**, 309 (2017).
- [45] H. Li, Y. Liu, and G. Long, *Sci China Phys Mech.* **60**, 080311 (2017).
- [46] Y. Xu, W. Cai, Y. Ma, X. Mu, L. Hu, T. Chen, H. Wang, Y. P. Song, Z.-Y. Xue, Z.-q. Yin, and L. Sun, *Phys. Rev. Lett.* **121**, 110501 (2018).
- [47] V. O. Shkolnikov and G. Burkard, (2018), [arXiv:1810.00193](https://arxiv.org/abs/1810.00193).
- [48] V. O. Shkolnikov, R. Mauch, and G. Burkard, (2019), [arXiv:1908.08443](https://arxiv.org/abs/1908.08443).
- [49] Z. Zhu, T. Chen, X. Yang, J. Bian, Z.-Y. Xue, and X. Peng, *Phys. Rev. Appl.* **12**, 024024 (2019).
- [50] T. Yan, B.-J. Liu, K. Xu, C. Song, S. Liu, Z. Zhang, H. Deng, Z. Yan, H. Rong, K. Huang, *et al.*, *Phys. Rev. Lett.* **122**, 080501 (2019).
- [51] D. J. Egger, M. Ganzhorn, G. Salis, A. Fuhrer, P. Mueller, P. K. Barkoutsos, N. Moll, I. Tavernelli, and S. Filipp, *Phys. Rev. Appl.* **11**, 014017 (2019).
- [52] E. Sjöqvist, *Int. J. Quantum Chem.* **115**, 1311 (2015).
- [53] V. A. Mousolou, C. M. Canali, and E. Sjöqvist, *New J. Phys.* **16**, 013029 (2014).
- [54] V. Azimi Mousolou, *Phys. Rev. A* **96**, 012307 (2017).
- [55] V. A. Mousolou, *EPL* **121**, 20004 (2018).
- [56] V. Azimi Mousolou, *Phys. Rev. A* **98**, 062340 (2018).
- [57] Y.-H. Kang, Z.-C. Shi, B.-H. Huang, J. Song, and Y. Xia, *Phys. Rev. A* **101**, 032322 (2020).
- [58] V. A. Mousolou, *EPL* **117**, 10006 (2017).
- [59] C. Wang and Z. Guo, *EPL* **124**, 40003 (2018).
- [60] M. Tian, Z. W. Barber, J. A. Fischer, and W. R. Babbitt, *Phys. Rev. A* **69**, 050301(R) (2004).
- [61] H. Imai and A. Morinaga, *Phys. Rev. A* **76**, 062111 (2007).
- [62] A. J. Sigillito, M. J. Gullans, L. F. Edge, M. Borselli, and J. R. Petta, (2019), [arXiv:1906.04512](https://arxiv.org/abs/1906.04512).
- [63] K. Takeda, A. Noiri, J. Yoneda, T. Nakajima, and S. Tarucha, (2019), [arXiv:1910.00771](https://arxiv.org/abs/1910.00771).
- [64] D. J. van Woerkom, P. Scarlino, J. H. Ungerer, C. Müller, J. V. Koski, A. J. Landig, C. Reichl, W. Wegscheider, T. Ihn, K. Ensslin, and A. Wallraff, *Phys. Rev. X* **8**, 041018 (2018).
- [65] J. M. Fink, R. Bianchetti, M. Baur, M. Göppl, L. Steffen, S. Filipp, P. J. Leek, A. Blais, and A. Wallraff, *Phys. Rev. Lett.* **103**, 083601 (2009).
- [66] J. Zhou, B. Liu, Z. Hong, and Z. Xue, *Sci China Phys Mech.* **61**, 010312 (2018).
- [67] J. Romhányi, G. Burkard, and A. Pályi, *Phys. Rev. B* **92**, 054422 (2015).
- [68] F. Yan, S. Gustavsson, J. Bylander, X. Jin, F. Yoshihara, D. G. Cory, Y. Nakamura, T. P. Orlando, and W. D. Oliver, *Nat. Commun.* **4**, 2337 (2013).
- [69] N. Didier, E. A. Sete, J. Combes, and M. P. da Silva, *Phys. Rev. Appl.* **12**, 054015 (2019).
- [70] F. Motzoi and F. K. Wilhelm, *Phys. Rev. A* **88**, 062318 (2013).
- [71] E. Knill, D. Leibfried, R. Reichle, J. Britton, R. B. Blakestad, J. D. Jost, C. Langer, R. Ozeri, S. Seidelin, and D. J. Wineland, *Phys. Rev. A* **77**, 012307 (2008).
- [72] E. Magesan, J. M. Gambetta, and J. Emerson, *Phys. Rev. A* **85**, 042311 (2012).
- [73] C. Zhang, X.-C. Yang, and X. Wang, *Phys. Rev. A* **94**, 042323 (2016).
- [74] C. Zhang, R. E. Throckmorton, X.-C. Yang, X. Wang, E. Barnes, and S. Das Sarma, *Phys. Rev. Lett.* **118**, 216802 (2017).
- [75] F. A. Calderon-Vargas and J. P. Kestner, *Phys. Rev. B* **91**, 035301 (2015).
- [76] Y. Makhlin, *Quantum Inf. Process* **1**, 243 (2002).